Pattern formation in weakly forced Taylor-Couette flow

Zhenyu Li and Roger E. Khayat*
Department of Mechanical and Materials Engineering, The University of Western Ontario, London, Ontario, Canada N6A 5B9
(Received 15 October 2003; published 27 April 2004)

Low-inertia vortex formation and pattern selection are examined for axisymmetric Taylor-Couette flow with spatially modulated cylinders. The forcing is arbitrary but remains periodic. The modulation amplitude is assumed to be small, and a regular perturbation expansion is used to determine the flow field at small to moderately large Taylor numbers (below the critical threshold). It is found that the presence of a weak modulation leads unambiguously to the emergence of steady Taylor-vortex flow even at vanishingly small Taylor number. This situation is closely reminiscent of the effect of end plates, and the consequent onset of imperfect bifurcation. The vortex structure is found to have the same periodicity as the forcing when only one of the cylinders is modulated, or when the modulations are commensurate. For incommensurate modulations, the vortex pattern is quasiperiodic, with regions of almost purely azimuthal flow. When the counter-rotation speed of the outer cylinder increases, the original vortices are gradually replaced by new ones that end up spanning the entire gap width, and in turn break up into two vortices resulting in two rows of vortices commensurate with each cylinder modulation. It is also shown that, for any modulation amplitude, the forcing wave number that generates the most intense vortex flow for a given Taylor number varies monotonically with Ta, but always reaches the critical value predicted by linear stability analysis for straight cylinders, regardless of which cylinder is modulated.

DOI: 10.1103/PhysRevE.69.046305 PACS number(s): 47.32.Cc

I. INTRODUCTION

While the Taylor-Couette flow (TCF) between straight cylinders has been extensively investigated [1,2], little attention has been devoted to the flow between two spatially modulated cylinders. The present theoretical study reports on an extensive range of interesting phenomena and mechanisms resulting from spatial modulation, which are closely related to phenomena encountered in other systems, namely, thermal convection [3]. Vortex formation and pattern selection at low to moderately large Taylor numbers is emphasized. The spatial modulation of the inner and/or outer cylinder is closely analogous to the presence of end effects in TCF; in both cases the forcing makes itself felt at precritical values of the Taylor number Ta_c. It is well established that vortices adjacent to the end plates form far below Ta_c [1,4]. When the precritical Taylor number is gradually increased, additional vortices are formed on top of each other until the vortices coming from the (symmetric) top and bottom plates meet in the middle of the column, at the critical Taylor number predicted by linear analysis. The number of vortices depends on the length of the cylinder. The presence of end plates for finite cylinder length is equivalent to imposing a strong modulation of wavelength equal to the length of the cylinder. It is important to observe that cell formation is spontaneous in the presence of end effects, and occurs at any rotational speed [1].

Ikeda and Maxworthy [5] carried out visualization experiments on spatially forced Taylor-vortex flow (TVF). Only the inner cylinder was modulated. Many of the complex phenomena observed in the unforced case were observed for the forced flow. However, the natural frequency, corresponding to the onset of TVF between straight cylinders, did not seem to appear in their system, at least under the flow conditions used in their experiment. It was found that the forcing fixes the size of the vortices, but vortex flow is only observed once Ta exceeds Ta_c. These findings seem to contradict the earlier observations of Koschmieder [6], who considered the effect of forcing caused by O-rings wrapped at regular intervals around the inner cylinder. Vortex flow was discerned very early. The first photograph showing signs of vertical activity along the entire column was taken at $\mathrm{Ta}=0.03\ \mathrm{Ta}_c$. Increasing the angular velocity steadily intensified the vortex flow. The sinks, the location of radial inward flow at the outer cylinder, became prominent as steady perfectly horizontal lines. The sources, the locations of radial outward flow at the outer cylinder were not distinct. The distance from sink to sink or the size of the forced vortex pair was equal to the forcing wavelength. However, in contrast to the observations in the narrow-gap limit, the sinks were not at a location symmetric about the O-rings; rather the location of the O-rings is 25% upward from the lower sink of each vortex pair. The occurrence of the sources at the location of the O-rings is of course expected, given the stronger centrifugal effect at that level. More recently, Painter and Behringer [7] also examined experimentally the effect of cylinder modulation, and, unlike Ikeda and Maxworthy [5], they did observe vortex flow at low Ta, but not as low as in Koschmieder's [6] experiment. Although it is well known that the Taylor number required for the instability to develop in unforced TCF is smaller for larger gap width, the discrepancy between the two experiments could not be attributed to the narrow-gap apparatus used by Ikeda and Maxworthy [5]. The present theoretical study clarifies the origin of the discrepancies among earlier experiments, and reports on the conditions for

*Corresponding author. Email address: rkhayat@eng.uwo.ca; URL:http://www.engga.uwo.ca/people/rkhayat

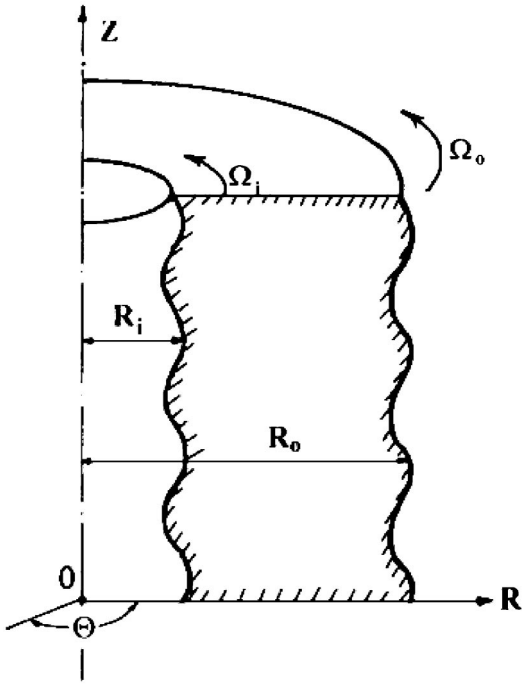

FIG. 1. Schematic of Taylor-vortex flow with weakly spatial modulation.

emergence and structure of low Taylor-number secondary flow as a result of cylinder modulation. A perturbation approach will be used to generate the flow for weakly corrugated cylinders. This approach has successfully been implemented and validated for the nonlinear flow [8] and heat transfer [9] in spatially modulated structures. It will be shown that the presence of negligibly small modulation is sufficient to induce a drastic departure from the (purely azimuthal) TCF. In other words, the forcing destabilizes the TCF.

II. PROBLEM FORMULATION

In this section, the general equations and boundary conditions for the Taylor-Couette flow with modulated cylinder walls is derived in the narrow-gap limit. After mapping the equations over the rectangular domain, a regular perturbation expansion for the flow field is carried out for weak modulation.

A. Governing equations in the narrow-gap limit

Consider the steady flow of an incompressible Newtonian fluid between two concentric infinite cylinders, as shown in Fig. 1. Both cylinders are assumed to be periodically modulated along the axial direction Z. The inner and outer cylinders are assumed to rotate at constant angular velocities, Ω_i and Ω_o, respectively. The inner cylinder is taken to always rotate counter clockwise, so that $\Omega_i > 0$. Thus, Ω_o may be positive, zero, or negative.

The general conservation of mass and linear momentum equations are, respectively,

$$\nabla \cdot \mathbf{U} = 0, \tag{1}$$

$$\frac{\partial \mathbf{U}}{\partial t} + \mathbf{U} \cdot \nabla \mathbf{U} = \nu \nabla^2 \mathbf{U} - \frac{1}{\rho} \nabla P, \tag{2}$$

where $\mathbf{U} = (\mathbf{U}_R, \mathbf{U}_\Theta, \mathbf{U}_Z)^T$ is the velocity vector in the cylindrical coordinates (R, Θ, Z) with Z taken along the common cylinder axis, P is the pressure, ν the kinematic viscosity, ρ the density, ∇ the three-dimensional gradient operator, and ∇^2 the Laplacian operator. The cylinders are assumed to be weakly modulated along the axial direction. Thus, the radii of the inner and outer cylinders, R_i and R_o, can be given by

$$R_i(Z) = \overline{R_i} + A_i F_i(Z), \tag{3}$$

$$R_o(Z) = \overline{R_o} + A_o F_o(Z), \tag{4}$$

where $\overline{R_i}$ and $\overline{R_o}$ are the mean radii of the inner and outer cylinders, respectively; A_i and A_o are the respective amplitudes of the modulation; $F_i(Z)$ and $F_o(Z)$ represent the shape functions of the modulation. The fluid is assumed to adhere to the cylinders, so that

$$U_R = U_Z = 0 \quad \text{and} \quad U_\Theta = \Omega_i R_i \quad \text{at } R = R_i, \tag{5}$$

$$U_R = U_Z = 0 \quad \text{and} \quad U_\Theta = \Omega_o R_o \quad \text{at } R = R_o. \tag{6}$$

The first step in reducing Eqs. (1) and (2) to the narrow-gap limit consists of introducing dimensionless coordinates, x and z, in the radial and axial directions, respectively, time t, pressure p, and velocity components u, v, w, as follows:

$$x = \frac{2R - (\overline{R_i} + \overline{R_o})}{2\overline{D}}, \quad z = \frac{Z}{\overline{D}}, \quad t = \frac{\nu}{\overline{D}},$$

$$p = \frac{\overline{D}^2}{\rho \nu} P, \quad u = \frac{\overline{D}}{\nu} U_R, \quad v = \frac{1}{R_i \Omega_i} U_\Theta, \quad w = \frac{\overline{D}}{\nu}, \tag{7}$$

where $\overline{D} = \overline{R_o} - \overline{R_i}$ is the mean gap width. Note that the ratio of mean gap width and inner cylinder radius is small (narrow-gap limit). After nondimensionlization, the conservation equations of steady-state TCF are reduced to the following form in the narrow-gap limit,

$$u_x + w_z = 0, \tag{8}$$

$$u u_x + w u_z = \mathrm{Ta}\, v^2 + u_{xx} + u_{zz} - p_x, \tag{9}$$

$$u v_x + w v_z = v_{xx} + v_{zz}, \tag{10}$$

$$u w_x + w w_z = w_{xx} + w_{zz} - p_z, \tag{11}$$

where a subscript denotes partial differentiation. The Taylor number Ta is defined in terms of the Reynolds number Re, and the average gap-to-radius ratio δ,

$$\mathrm{Ta} = \mathrm{Re}^2 \delta, \quad \mathrm{Re} = \frac{\overline{R_i} \Omega_i \overline{D}}{\nu}, \quad \delta = \frac{\overline{D}}{\overline{R_i}}. \tag{12}$$

Here the dimensionless physical domain is defined by $(x,z)\in[-1/2+\varepsilon f_i(z),1/2+\varepsilon f_o(z)]\times(-\infty,+\infty)$, where ε is a measure of the dimensionless modulation amplitude. In this work, the modulation amplitude is assumed to be small. Without loss of generality, the shape functions of the modulation of the inner and outer cylinders are taken as $f_i(z)=\Sigma_{n=1}^{N} f_n^i \sin(n\alpha z)$ and $f_o(z)=\Sigma_{n=1}^{N} f_n^o \sin(n\beta z+\phi)$, respectively, where α and β are the wave numbers of the modulations, ϕ is a phase angle, f_n^i and f_n^o are constant coefficients, and N is the number of modes. Thus, Ta, ε, α, β, ϕ, as well as the outer-to-inner cylinder velocity ratio, $\omega=\Omega_o/\Omega_i$, are the important parameters in the present problem.

B. Domain mapping and numerical solution

Equations (8)–(11) are solved by first mapping the physical domain in the (x,z) plane onto a rectangular domain $(\eta,\xi)\in[-1/2,1/2]\times(-\infty,+\infty)$, which is given by

$$\xi = z, \tag{13}$$

$$\eta = \frac{x}{1-\varepsilon[f_i(z)-f_o(z)]} - \frac{\varepsilon[f_i(z)+f_o(z)]}{2-2\varepsilon[f_i(z)-f_o(z)]}, \tag{14}$$

where $\xi\in[-\infty,+\infty]$ and $\eta\in[-1/2,1/2]$. The governing equations in mapped domain become

$$u_\eta + [1-\varepsilon(f_i-f_o)]w_\xi + \varepsilon\left[\eta(f_{i\xi}-f_{o\xi}) - \tfrac{1}{2}(f_{i\xi}+f_{o\xi})\right]w_\eta = 0, \tag{15}$$

$$\begin{aligned}
&[1-\varepsilon(f_i-f_o)]uu_\eta + [1-\varepsilon(f_i-f_o)]^2 wu_\xi + \varepsilon[1-\varepsilon(f_i-f_o)]\left[\eta(f_{i\xi}-f_{o\xi}) - (f_{i\xi}+f_{o\xi})\tfrac{1}{2}\right]wu_\eta \\
&\quad = \mathrm{Ta}[1-\varepsilon(f_i-f_o)]^2 v^2 + u_{\eta\eta} + [1-\varepsilon(f_i-f_o)]^2 u_{\xi\xi} + \Big\{\varepsilon[1-\varepsilon(f_i-f_o)](f_{i\xi\xi}-f_{o\xi\xi})\eta + 2\varepsilon^2(f_{i\xi}-f_{o\xi})^2\eta - \tfrac{\varepsilon}{2}[1-\varepsilon(f_i-f_o)] \\
&\qquad \times(f_{i\xi\xi}+f_{o\xi\xi}) - \varepsilon^2(f_{i\xi}^2-f_{o\xi}^2)\Big\}u_\eta + 2\varepsilon[1-\varepsilon(f_i-f_o)]\left[\eta(f_{i\xi}-f_{o\xi}) - (f_{i\xi}+f_{o\xi})\tfrac{1}{2}\right]u_{\eta\xi} \\
&\qquad + \varepsilon^2\left[\eta^2(f_{i\xi}-f_{o\xi})^2 - \eta(f_{i\xi}^2-f_{o\xi}^2) + (f_{i\xi}+f_{o\xi})^2\tfrac{1}{4}\right]u_{\eta\eta} - [1-\varepsilon(f_i-f_o)]\,p_\eta,
\end{aligned} \tag{16}$$

$$\begin{aligned}
&[1-\varepsilon(f_i-f_o)]uv_\eta + [1-\varepsilon(f_i-f_o)]^2 wv_\xi + \varepsilon[1-\varepsilon(f_i-f_o)]\left[\eta(f_{i\xi}-f_{o\xi}) - (f_{i\xi}+f_{o\xi})\tfrac{1}{2}\right]wv_\eta \\
&\quad = v_{\eta\eta} + [1-\varepsilon(f_i-f_o)]^2 v_{\xi\xi} + 2\varepsilon[1-\varepsilon(f_i-f_o)]\left[\eta(f_{i\xi}-f_{o\xi}) - (f_{i\xi}+f_{o\xi})\tfrac{1}{2}\right]v_{\eta\xi} + \Big\{\varepsilon[1-\varepsilon(f_i-f_o)](f_{i\xi\xi}-f_{o\xi\xi})\eta \\
&\qquad + 2\varepsilon^2(f_{i\xi}-f_{o\xi})^2\eta - \tfrac{\varepsilon}{2}[1-\varepsilon(f_i-f_o)]\,(f_{i\xi\xi}+f_{o\xi\xi}) - \varepsilon^2(f_{i\xi}^2-f_{o\xi}^2)\Big\}v_\eta + \varepsilon^2\left[\eta^2(f_{i\xi}-f_{o\xi})^2 - \eta(f_{i\xi}^2-f_{o\xi}^2)\right. \\
&\qquad \left. + (f_{i\xi}+f_{o\xi})^2\tfrac{1}{4}\right]v_{\eta\eta},
\end{aligned} \tag{17}$$

$$\begin{aligned}
&[1-\varepsilon(f_i-f_o)]uw_\eta + [1-\varepsilon(f_i-f_o)]^2 ww_\xi + \varepsilon[1-\varepsilon(f_i-f_o)]\left[\eta(f_{i\xi}-f_{o\xi}) - \tfrac{1}{2}(f_{i\xi}+f_{o\xi})\right]ww_\eta \\
&\quad = w_{\eta\eta} + [1-\varepsilon(f_i-f_o)]^2 w_{\xi\xi} - [1-2\varepsilon(f_i-f_o)+\varepsilon^2(f_i-f_o)^2]\,p_\xi + \Big\{\varepsilon[1-\varepsilon(f_i-f_o)]\,(f_{i\xi\xi}-f_{o\xi\xi})\eta + 2\varepsilon^2(f_{i\xi}-f_{o\xi})^2\eta \\
&\qquad - \tfrac{\varepsilon}{2}[1-\varepsilon(f_i-f_o)](f_{i\xi\xi}+f_{o\xi\xi}) - \varepsilon^2(f_{i\xi}^2-f_{o\xi}^2)\Big\}w_\eta + 2\varepsilon[1-\varepsilon(f_i-f_o)]\left[\eta(f_{i\xi}-f_{o\xi}) - \tfrac{1}{2}(f_{i\xi}+f_{o\xi})\right]w_{\eta\xi} \\
&\qquad + \varepsilon^2\left[\eta^2(f_{i\xi}-f_{o\xi})^2 - \eta(f_{i\xi}^2-f_{o\xi}^2) + \tfrac{1}{4}(f_{i\xi}+f_{o\xi})^2\right]w_{\eta\eta} - \varepsilon[1-\varepsilon(f_i-f_o)]\left[\eta(f_{i\xi}-f_{o\xi}) - \tfrac{1}{2}(f_{i\xi}+f_{o\xi})\right]p_\eta.
\end{aligned} \tag{18}$$

The mapping allows ε to emerge as the perturbation parameter in the transformed equations, and a regular perturbation expansion is sought for the velocity and pressure, which can be written as

$$\begin{aligned}
X(\eta,\xi) &= X_0(\eta,\xi) + \varepsilon\sum_{n=1}^{N}\left[X_n^i(\eta)e^{in\alpha\xi} + X_n^o(\eta)e^{i(n\beta\xi+\phi)}\right] \\
&\quad + \text{c.c.} + O(\varepsilon^2),
\end{aligned} \tag{19}$$

where $X=(u,v,w,p)$, and c.c. represents the complex conjugate part. The superscripts i and o denote the effects associated with the spatial modulation at the inner and outer cylinder, respectively. To leading order in ε, one recovers the equations that correspond to the flow between two straight cylinders, namely,

$$u_0(\eta,\xi) = w(\eta,\xi) = 0, \tag{20a}$$

$$v_0(\eta,\xi) = \frac{\omega+1}{2} + (\omega-1)\eta, \tag{20b}$$

$$p_0(\eta,\xi) = \mathrm{Ta}\left(\tfrac{7}{12}\omega^2 + \tfrac{5}{6}\omega + \tfrac{7}{12}\right). \tag{20c}$$

To $O(\varepsilon)$, the continuity and momentum conservation equations reduce to a set of $8N$ nonhomogeneous ODEs, with the

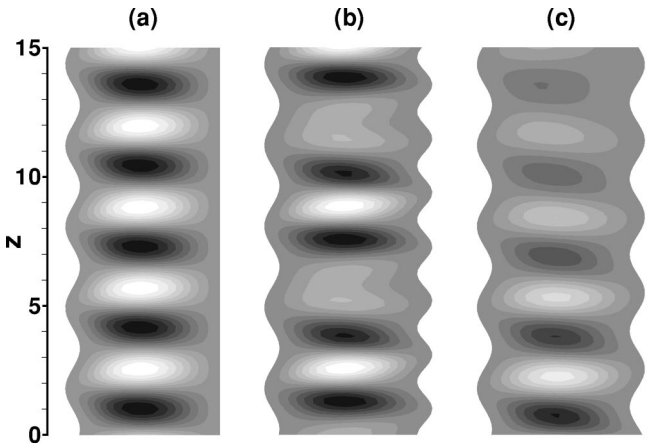

FIG. 2. Cross-sectional view of vortex flow for $\alpha=2$, $\omega=0$, and $\beta=$(a) 0,(b) 3,(c) 2.13.

forcing appearing as the nonhomogeneity. Then the set of ODEs are solved subject to homogeneous boundary conditions. The problem is of the two-boundary-value type. A variable-step finite-difference scheme is used to obtain the solution. The basic discretization used is the trapezoidal rule over a nonuniform mesh. This mesh is chosen adaptively, to make the local error approximately the same size everywhere. Higher-order discretizations are obtained by differed corrections and global error estimates are produced to control the computation. The resulting algebraic system is solved by a special form of Gauss elimination that preserves sparseness.

III. RESULTS AND DISCUSSION

Consider first the situation when only the inner cylinder is rotated, which is illustrated in Fig. 2 for three different configurations, when only the inner cylinder is modulated ($\beta=0$), and when the modulations are commensurate ($\beta=3$), and incommensurate ($\beta=2.13$). The corresponding signatures for $u(x=0,z)$ are depicted from Fig. 3. Here $\varepsilon=0.05$, $\alpha=2$, and Ta=500. Both modulations at the inner and outer cylinders are sinusoidal. Note that dark (light) areas indicate vortices in the clockwise (counter-clockwise) direction. The mean range in the radial direction is $[-1/2,+1/2]$. When only the inner cylinder is modulated ($\beta=0$), there is a pair of vortices that span the entire gap width, extending over a modulation wavelength. The flow is spatially periodic in z of the linear type as Fig. 3(a) indicates. Similarly to unforced TVF, it is found that the larger the gap width, the stronger is the secondary flow. Hence, it is expected that the maximum gap width along the axial direction initiates the production of the vortices. It is for this reason that the vortex flow preserves the same spatial periodicity when the outer cylinder is also modulated, as long as the modulations are commensurate [see Fig. 2(b)]. Analysis of the corresponding signature shows that the two basic wave numbers are clearly dominant, but higher harmonics are also evident. Spatial periodicity is lost when the two modulations are incommensurate, as illustrated by the $\beta=2.13$ flow. In this case, the flow pattern is

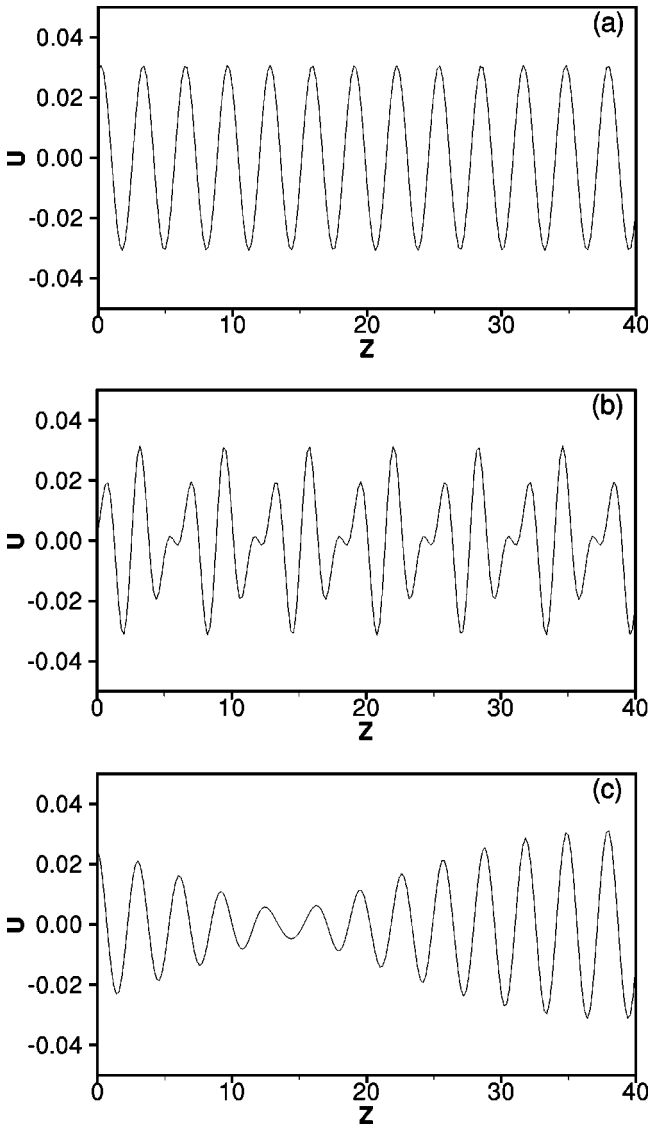

FIG. 3. Radial velocity profile u along the axial direction ($x=0$) for $\alpha=2.0$, $\beta=$(a) 0,(b) 3,(c) 2.13.

quasiperiodic, with vortex wave group appearing, with a wave number equal to the average of the cylinder wave numbers. Two successive groups are separated by zones of a rapid decay of the strength of vortices, leading to an almost purely azimuthal flow in these zones. The situation is reminiscent of the predictions of Eagles and Eames [10] for slowly varying cylinders (see their Figs. 2 and 3). It is generally observed that for a modulated and rotating inner cylinder, the number of vortices does not depend on the modulation of the outer cylinder.

Clearly, the effect of the forcing can be examined by varying the amplitude and wavelength of the modulation. For sinusoidal forcing as in Fig. 2, only the intensity and not the pattern of the flow is affected by ε and Ta. For a straight outer cylinder, the wavelength of the vortex flow is found to be always equal to the wavelength of the inner cylinder, as was also observed in experiments involving sinusoidal forcing [5,10]. This is in analogy with the flow inside a gap with spatially ramped end condition. It was shown, both theoreti-

cally [11] and experimentally [12], that the ramped flow reduces the accessible wavelength compared with the unramped case in which the wavelength depends on the length of the section. However, unlike the ramped sections, which result in a constraint leading to wavelength at or near the natural wavelength, only the forced wavelength is predicted by the present calculations, at least regarding the secondary vortices. Ikeda and Maxworthy [5] were not able to obtain the natural wavelength in their system, and rightly attributed this inability to relatively large modulation amplitude of the forcing (10 % of the gap width). Indeed, the present small-amplitude formulation clearly demonstrates that the only solution admitted by the flow equations must be commensurate with the sinusoidal forcing wavelength.

The discrepancy between the results of Koschmieder [6] and those of Ikeda and Maxworthy [5] can now be understood in the light of the present calculations. Recall that the latter authors did not observe secondary flow at small Taylor number. Inspection of the conservation equations in the narrow-gap limit clearly indicates that secondary flow is bound to emerge at a nonvanishing Taylor number when modulation is present. The modulation forces the azimuthal velocity to depend on the axial coordinate z. Subsequently, the centrifugal term in the radial momentum equation ensures the dependence of the pressure on axial position, which in turn results in a nonvanishing axial (and radial) flow. Thus, unless curvature effects vanish completely, one should expect secondary flow to emerge at any Taylor number, as depicted from Fig. 2. In other words, and similarly to the situation when end plates are fixed to a stationary outer cylinder, the wall modulation exercises a constraint on the flow developed by rotation of the inner cylinder. In particular, near the peaks of the wall modulation, a negative centrifuging force drives the fluid radially outwards. Consequently, a circulation is necessary in the meridional plane, and the flow cannot be purely circumferential, as it is for a flow between infinite straight cylinders. From a nonlinear point of view, the spontaneous onset of vortex flow at any precritical Taylor number, is equivalent to the onset of an imperfect bifurcation, reflecting a smooth transition, instead of the supercritical (pitchfork) bifurcation predicted for a flow between straight cylinders [4]. In the experiment of Ikeda and Maxworthy [5], the annular gap was filled with tap water and the flow was visualized by the addition of 2% by volume Kalliroscope solution, which consisted of guanine flakes that were used to visualize the flow since the flakes spend more time aligned with the shear of the flow than they spend rotating. Moreover, these reflective flakes are almost neutrally buoyant. In laminar flow, the flakes in the gap width align with the shear such that the spatial modulations on the inner cylinder could barely be seen through the field of particles. It is thus possible that the tendency for the forcing to generate a secondary flow before the Taylor instability threshold was simply missed in the experiment. In other words, the secondary flow may very well exist in the precritical range, but it was too weak to be observed. Current calculations show that the level of radial and axial flow may remain orders of magnitude weaker than circumferential flow for Ta smaller than Ta_c. The flow regimes were identified in the experiment using only flow visualization and not (velocity) measurements.

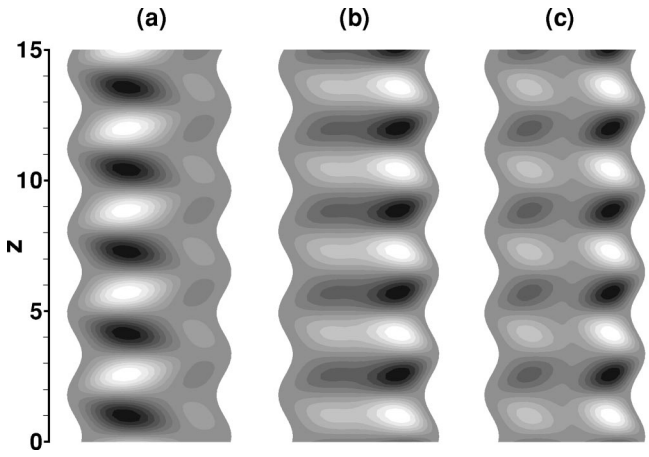

FIG. 4. Vortex breakup for $\alpha=\beta=2$, and $\omega=$(a) -0.8, (b) -12, (c) -20.

Ikeda and Maxworthy [5] reported a scatter in their data, which they attributed to the difficulty in visualizing the vortices when there is only slight vertical motion.

A similar flow pattern is also predicted (not shown) when only the outer cylinder is modulated. In this case, and similarly to Fig. 2, the outflow of the vortex pair always occurs at the peak of the sine wave modulation, i.e., at the minimum gap width. This is of course expected because the centrifugal force on a particle is larger at the peaks than at the troughs of the modulation of the cylinder. Here too, the external forcing dominates the size of the vortices, and only the forced wavelength appears in the system. Whether there exists a level of forcing at which the forcing wavelength would cease to dominate the flow is an important issue, which could not be addressed in the previous experiments. The current calculations show that varying the amplitude and wavelength of the forcing leads to a flow response that is always commensurate with the forcing, and only one vortex pair is present in a spatial period, as in Fig. 2.

When the outer cylinder is counter rotated, an additional vortex pair appears, the strength of which depends on the counter-rotation speed ω. The situation is illustrated in Fig. 4 for $\mathrm{Ta}=500$, $\varepsilon=0.05$, with $\alpha=\beta=2$. As ω departs from zero, the vortices [in Fig. 2(b)], which initially span the whole of the gap width, begin to shrink in width, but remain entirely commensurate with the inner cylinder modulation [Fig. 4(a)], with the vortex center shifting toward the inner cylinder. Simultaneously, secondary vortices form, originating at the outer cylinder, which grow at the expense of the original vortices, as ω increases. The original sinks and sources at the inner cylinder do not change their locations, even when the outer cylinder speed is further increased. At the outer cylinder, a new sink (source) forms where the source (sink) was originally, such that a saddle point forms between the two cylinders as shown in Fig. 4(a) for $\omega=-0.8$. The newly formed vortex pairs strengthen and increase in size, at the expense of the original vortex pairs, as the outer cylinder speed increases further. In other words, the original forced pairs were unstable and began to transform into two pairs of vortices. Initially, the newly formed pairs were weak and narrow, but they intensify steadily with increased counter-

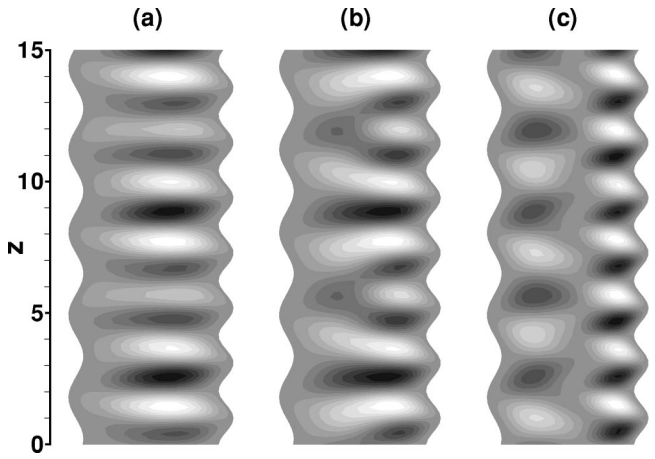

FIG. 5. Vortex breakup for $\alpha=2$, $\beta=3$, and $\omega=$(a)-2,(b) -5,(c)-20.

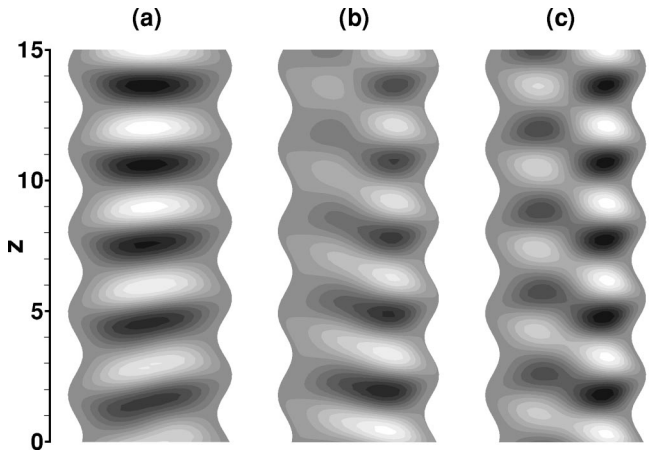

FIG. 6. Vortex breakup for $\alpha=2$, $\beta=2.13$, and $\omega=$(a)-1,(b) -5,(c)-10.

rotating speed. It is important to observe that both the primary and secondary vortices intensify with ω. However, the primary vortices begin to lose strength as is further increased, while they continue to shrink in size. At approximately $\omega=-5$, the primary vortices disappear entirely, and one recovers the situation for $\omega=0$ as the vortices span the entire gap width, except that the circulation is now in the opposite direction.

It is interesting to also note that the number of vortex pairs is the same as when $\omega=0$. As ω increases further, there is a relative strengthening (weakening) of vortex flow activity near the outer (inner) cylinder. Although the vortices still span the gap width, there is a break in the symmetry with respect to $x=0$, with the vortex center shifting toward the outer cylinder. The situation is illustrated in Fig. 4(b) for $\omega=-12$. New vortex pairs begin to appear near the inner cylinder, which gain in strength with ω, leading to the pattern shown in Fig. 4(c) for $\omega=-20$. This pattern seems to persist for higher ω. The sequence involving the breakup of the original vortex pairs and the emergence of the subpairs at the outer cylinder is a continuous process in which no critical counter-rotation speed exists.

The influence of ω on the flow when the modulations of the inner and outer cylinders are different is typically illustrated in Fig. 5, for $\alpha=2$ and $\beta=3$. The starting point is the case $\omega=0$ [shown in Fig. 4(b)], where the vortex pattern is commensurate with the inner cylinder modulation. Similar to the case in Fig. 4, the original vortices are replaced by new vortices as increases, as depicted from Fig. 5(a) for $\omega=-2$. The vortex pattern is now commensurate with the outer cylinder modulation. As ω increases further, the vortices break up as in Fig. 4. However, two new observations can be made relative to before, which are reflected in Fig. 5(a) for $\omega=-5$. First, not all vortices break up simultaneously, since some are stronger than others [as is evident from Fig. 5(a)]. The weaker vortices tend to break up first. Second, before breakup, the vortex tends to stretch typically between a valley at the outer cylinder and a valley at the inner cylinder. Thus, only one of two new resulting vortex pair remains at the same z level; the other vortex is drawn into the valleys of the inner cylinder. As increases further, the new vortices align themselves periodically in a manner that is commensurate with the inner and outer cylinders, as shown in Fig. 5(c) for $\omega=-20$. A similar sequence is predicted when the modulations are incommensurate; for example, when $\alpha=2$, $\beta=2.13$, as shown in Fig. 6 for $\omega=-1,-5$, and -10, respectively. Although in this case the breakup sequence is somewhat disorderly, the end pattern is very similar to that shown in Fig. 5(c) for $\omega=-20$. In particular, the flow appears to be helicoidal at small (see Fig. 6(a), for instance). However, as the counter-rotation speed increases, the flow breaks up into two series of vortices that span each cylinder.

Additional calculations were carried out to assess the influence of the spatial forcing as Ta approaches Ta_c. Linear stability analysis indicates that, for narrow-gap flow when the outer cylinder is at rest, Taylor vortices set in at a critical Taylor number, $\mathrm{Ta}_c=1690$ and a wave number equal to 3.13 [4]. Figure 7 displays the behavior of the modulation wave number α_m of the inner or β_m of the outer cylinder, which corresponds to the maximum vortex flow intensity, as function of Ta, for different modes of external forcing. The re-

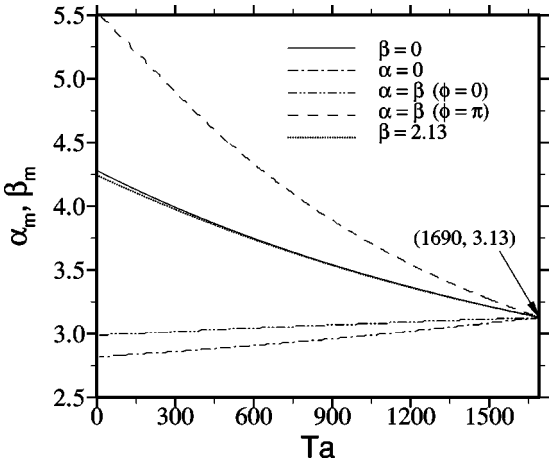

FIG. 7. Influence of inertia on pattern selection ($\omega=0$). The figure shows the dependence on *Ta* of the forcing wave number, α_m or β_m, which gives the strongest vortex flow for different cylinder modulations.

sults are found to be entirely independent of the modulation amplitude ε. This is an important observation as the results apply also to the limit of vanishingly small ε, emulating the flow between two straight cylinders. At a given Ta value, the wave number was varied until a value $\alpha=\alpha_m$ (or $\beta=\beta_m$ when only the outer cylinder is modulated) is found that corresponds to the maximum intensity in vertical flow. Different forcing levels were examined, corresponding to the modulation of the inner cylinder alone ($\beta=0$), the outer cylinder alone ($\alpha=0$), the in-phase ($\phi=0$), and out-of-phase ($\phi=\pi$) modulations of the cylinders. It is found, that in all four cases, α_m or β_m converges to the critical wave number 3.13 when Ta approaches 1690. This important result shows clearly the preference of the flow to approach the critical Taylor-vortex limit regardless of the type of forcing. Other forcing conditions were also considered, which lead to the same conclusion. One can confidently extrapolate this observation to any type of spatial modulation (in form, amplitude, and wavelength), particularly small modulations (roughness) that are always bound to emerge in practice on any cylinder surface. It is important to note that Fig. 6 does not indicate that the flow pattern corresponds to the natural TVF as Ta approaches Ta_c regardless of the forcing. The pattern is always dictated by the forcing.

The question regarding the different values of α_m (or β_m) for a given Ta can be explained on the basis of the balance theorem, which is generally used to understand the value of the wavelength under critical as well as supercritical conditions [1]. The theorem rests on the assumption that the averages in the velocity and pressure disturbances are zero. The discussion is further simplified if it is observed that the disturbance from azimuthal flow is small for small modulation amplitude. In this case, and under steady-state conditions, the balance theorem is achieved by contracting the momentum conservation equation with the velocity vector, and integrating over the gap. This leads to the balance between the average rate of centrifugal kinetic energy, and the average rate of viscous dissipation. The rate of dissipation is shown to be proportional to α^2. Thus, wide, short cells dissipate more energy than narrow, tall cells. Since, for a given Ta, centrifugal energy is stronger when the inner cylinder is not modulated, the wave number is expected to be higher. This explains the height of curve ($\beta=0$) relative to curve ($\alpha=0$) and the other curves in Fig. 7. This also means that all four curves cannot be parallel, and therefore should intersect. The solution of the Naiver-Stokes equations shows, unambiguously, that all four curves intersect precisely at the same point (1690, 3.13), corresponding to the critical threshold predicted by linear analysis. It is, however, important to mention that the results in Fig. 7 can be misleading as they may indicate that the perturbation theory is uniformly valid to include the critical point. At the critical point, the problem becomes degenerate and the regular perturbation expansion, Eq. (19), breaks down (see, for instance, Murdock [13]). The degeneracy of the problem can be readily recognized by examining the amplitude equation for the problem, as the forcing takes the form of an inhomogeneous perturbation term [see Eq. (2) in Painter and Behringer [7]].

In analogy with thermal convection [5,14], a singularity of $\mathrm{O}(\mathrm{Ta}-\mathrm{Ta}_c)^{-1}$ in flow amplitude is expected to emerge at the critical point. This can be seen more clearly from Fig. 8 where the magnitude of the maximum radial velocity U_{max} is examined as Ta approaches Ta_c for various values of α and β, where $\alpha_c=3.13$ represents the critical wave number for unmodulated flow. The curves in the figure illustrate three important classes of modulations. The solid curve corresponds to a modulation with both wave numbers equal to the critical value, that is, $\alpha=\beta=\alpha_c$, which reflects the highest magnitude in maximum velocity. This is expected because of the resonant wavelength excitation. Within the present regular perturbation approach, the modulation amplitudes are magnified according to the eigenvalues (growth rates) of the corresponding Fourier modes. Thus, the amplification of the mode corresponding to the critical wave number α_c diverges near $\mathrm{Ta}=\mathrm{Ta}_c$. The dashed curve with $\alpha=\beta=0.6\alpha_c$, corresponds to a modulation with both wave numbers different from the critical value, whereas the dash-dotted curve corresponds to $\alpha=\alpha_c$, $\beta=0.7\alpha_c$. It can be seen that the magnitude of the maximum radial velocity is strongly dependent upon the modulation wave numbers α and β. As the figure indicates, the maximum radial velocity increases in magnitudes as Ta increases and becomes singular when $\mathrm{Ta}=\mathrm{Ta}_c$ as long as the Fourier representation of the modulation contains a nonzero component with critical wave number α_c. Similar results were also obtained in thermal (Rayleigh-Bénard) convection problem with spatial periodic boundary conditions [3]. More importantly, the results show that the present approach remains valid when Ta is larger than Ta_c as long as the modulation wave numbers are different from the critical value.

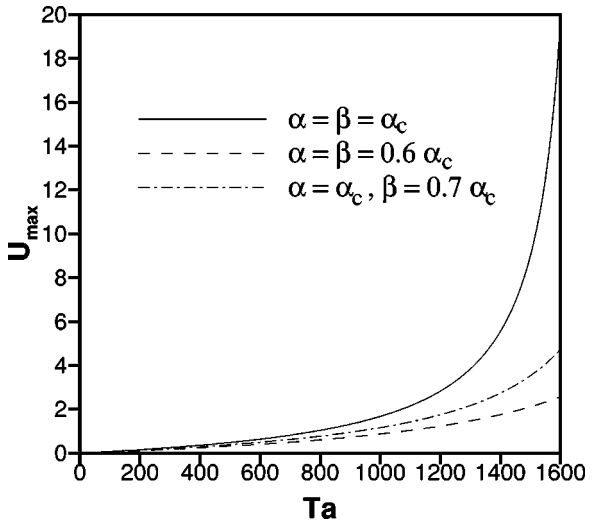

FIG. 8. Magnitude of the maximum radial velocity U_{max} as Ta approaching Ta_c for different modulation configurations.

Finally, the results reported so far are based on sinusoidal forcing, suggesting the existence of a strong correlation between the forcing and the ensuing vortex pattern. More importantly, the pattern does not change when Ta increases; it simply intensifies with Ta. Koschmieder [6] observed that this is not the case in the presence of O-rings. Note that the outer cylinder was kept at rest. Figure 9 depicts the response for the same forcing parameters as in the experiment, namely, the forcing amplitude $\varepsilon=0.17$ and the wavelength

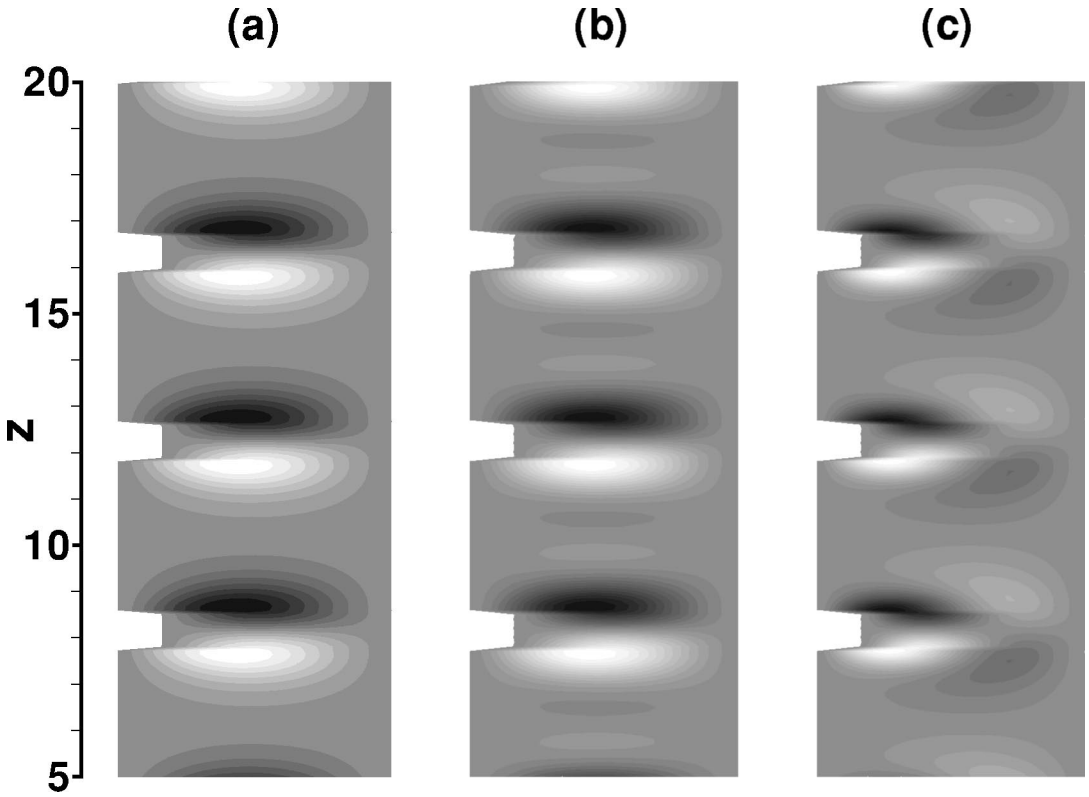

FIG. 9. Vortex formation for nonsinusoidal (O-ring) modulation of the inner cylinder ($\beta=0$), for the cases (a) $\mathrm{Ta}/\mathrm{Ta}_c=0.03$, $\omega=0$, (b) $\mathrm{Ta}/\mathrm{Ta}_c=0.48$, $\omega=0$, (c) $\mathrm{Ta}/\mathrm{Ta}_c=0.48$, $\omega=-1.35$.

$\lambda_f=2\pi/\alpha=4.09$ being about two times the critical wavelength $2\pi/\alpha_c$ for the onset of natural TVF. Koschmieder [6] reported that vortices were visible for Ta as low as 0.03 Ta_c. At this Taylor number, Fig. 9 shows the emergence of vortex pairs centered symmetrically about the O-rings. Unlike sinusoidal forcing [see Fig. 2(a)], the vortices do not occupy the whole modulation wavelength, although the number of vortex pairs is equal to the number of O-rings (per unit axial length), similarly to the experiment. While the vortex pairs were not centered about the O-rings in their experiment, which is probably due to end effects, the governing equations clearly do not allow a break in axial symmetric under symmetric forcing. Similarly to the experiment, and paraphrasing Koschmieder [6], Fig. 9 and additional calculations show that increasing the Taylor number further causes a new sink to appear gradually in between the two original sinks [see Fig. 9(b)], which mark the formation of new forced vortex pair. The location of the original sinks does not change as Ta increases. The appearance of the new sinks signals the formation of a new vortex pair within each original vortex pair. Koschmieder [6] observed rightly "the original forced pairs were unstable and began to transform into two pairs of vortices." The present calculations also show that "initially, the newly formed subpairs were weak and narrow, but they intensified steadily with increased Taylor number." The predicted wavelength (per unit gap width) of the subpairs in Fig. 9 is 1.60 while the larger pairs have a wavelength equal to 2.49. Koschmieder [6] (see his Fig. 1 and corresponding text) reported the wavelengths of the subpairs and larger pairs to be 1.61 and 2.46, respectively. It is interesting to observe that the emergence of the vortex subpairs does not always occur. In fact, similarly to Koschmieder's experiment [6], it is found that a critical forcing wavelength (spacing between two successive O-rings) is needed for the original vortices to destabilize.

Counter rotation leads to complex patterns that depend on Ta. The discussion is limited here to the case $\mathrm{Ta}/\mathrm{Ta}_c=0.48$. As ω increases from zero, the vortex subpair weakens and disappears completely, reverting the situation back to that in Fig. 9(a). The original vortices in turn weaken as ω increases further. Simultaneously, a new vortex pair (opposite in sense) is initiated at the outer cylinder, which gains strength with counter-rotation speed, as illustrated in Fig. 9(c). The process of vortex disappearance and birth continues as ω increases further.

IV. CONCLUSION

The onset of low-inertia vortex flow in weakly modulated TCF is addressed in this study. The work is of fundamental importance as it is related to pattern formation in other systems. A symmetry-breaking transition occurs, which is due to the spatial forcing that couples directly to the new mode, driving this mode with increasing strength and approaching the onset point. Both cylinders can be arbitrarily modulated, and the influences of both commensurate and incommensurate modulations, as well the effect of counter rotation are explored. Various vortex flow patterns are found when the purely azimuthal flow is perturbed. In this case, the pattern is always dictated by the forcing, when only one cylinder is

modulated. A quasiperiodic vortex pattern is predicted when the modulations are incommensurate. When the outer cylinder is counter rotated ($\omega<0$), the original vortices break up, leading to rows of vortices commensurate with each cylinder. Unlike the pattern after breakup, the breakup process itself depends strongly on the type of forcing. It is also verified that the wave number of the forcing that gives the most intense vortex flow approaches α_c as Ta approaches Ta_c (from below and above). This result may also be understood within the amplitude equation formalism of Newell and Whitehead [15]. Direct comparison with the measurements of Koschmieder [6] for O-ring forcing led to good agreement.

In conclusion, the proposed formulation and reported results illustrate how the onset, breakup, and formation of vortex patterns can be predicted and controlled to any degree of accuracy and refinement. Unlike TVF, where vortex formation is spontaneous, the vortex pattern for modulated TCF is completely predictable once a forcing modulation is imposed. The study helps elucidate the origin of the discrepancies among earlier experiments on low-inertia vortex formation, and constitutes a reliable guide for future experiments. All vortex patterns reported are stable, as they are the only solution to the flow equations. These patterns are therefore expected to always exist in reality. However, calculations show that their observability depends strongly on their intensity.

ACKNOWLEDGMENT

The financial support of the Natural Science and Engineering Research Council is gratefully acknowledged.

[1] E. L. Koschmieder, *Bénard Cells and Taylor Vortices* (Cambridge University Press, London, 1992).
[2] R. Tagg, Nonlinear Sci. Today **4**, 1 (1994).
[3] R. E. Kelly and D. Pal, J. Fluid Mech. **86**, 433 (1978).
[4] J. T. Stuart, SIAM Rev. **28**, 315 (1986).
[5] E. Ikeda and T. Maxworthy, Phys. Rev. E **49**, 5218 (1994).
[6] E. L. Koschmieder, Phys. Fluids **18**, 499 (1975).
[7] B. D. Painter and R. P. Behringer, Europhys. Lett. **44**, 599 (1998).
[8] H. Zhou, R. E. Khayat, R. J. Martinuzzi, and A. G. Straatman, Int. J. Numer. Methods Fluids **39**, 1139 (2002).
[9] M. R. Siddique and R. E. Khayat, Numer. Heat Transfer, Part A **43**, 481 (2003).
[10] P. M. Eagles and K. Eames, J. Eng. Math. **17**, 263 (1983).
[11] H. Riecke, Phys. Rev. A **37**, 636 (1988).
[12] L. Ning, G. Ahlers, and D. S. Cannell, Phys. Rev. Lett. **64**, 1235 (1990).
[13] J. A. Murdock, *Perturbations: Theory and Methods* (Wiley, New York, 1991).
[14] F. H. Busse, J. Fluid Mech. **52**, 97 (1972).
[15] A. C. Newell and J. A. Whitehead, J. Fluid Mech. **38**, 279 (1972).